



Characteristics of surface evapotranspiration and its response to climate and land use and land cover in the Huai River Basin of eastern China

Meng Li^{1,2} · Ronghao Chu³ · Abu Reza Md. Towfiqul Islam⁴ · Shuanghe Shen⁵

Received: 9 December 2019 / Accepted: 6 August 2020
© Springer-Verlag GmbH Germany, part of Springer Nature 2020

Abstract

The Huai River Basin (HRB) has experienced significant climate and land use and land cover changes (LUCC) which have impacted the water cycle in recent times. However, little is understood about the impact of climate change and LUCC affecting evapotranspiration (ET). Thus, we investigate how surface ET response to climate change and LUCC in the HRB for the period from 2001 to 2014. ET and land cover types products (i.e., MOD16 and MCD12Q1, respectively) from MODerate-resolution Imaging Spectroradiometer (MODIS) were employed in this research. Water balance method and D20 pan evaporation data (E_{pan}) as well as eddy covariance (EC) measurements were used to validate the MOD16 product, and the Theil–Sen's slope estimator and Mann–Kendall (M-K) test were adopted to estimate the magnitude and significance of ET trends. Moreover, daily meteorological data of 137 weather stations from 2001 to 2014 were also employed to explore the correlation mechanism between ET and meteorological factors. The results showed that the accuracy of MOD16 product data were convincing and could be used to estimate ET in the HRB. The higher values of ET are mainly distributed in the south and lower values in the north. ET decreased significantly in all seasons except in spring, especially in winter. The results also depicted that the land-use type in the HRB is mainly croplands, followed by forests and grasslands. Croplands area showed a decreasing trend at a rate of $-176.2 \text{ km}^2 \cdot \text{a}^{-1}$, grasslands area presents a w-type fluctuation decreasing trend with a rate of $-35.8 \text{ km}^2 \cdot \text{a}^{-1}$, urban/built-up area increased at a rate of $138.3 \text{ km}^2 \cdot \text{a}^{-1}$, water bodies area decreased gradually at a rate of $-1.38 \text{ km}^2 \cdot \text{a}^{-1}$, wetlands area increased significantly at a rate of $43.6 \text{ km}^2 \cdot \text{a}^{-1}$, and barren area decreased gradually at a rate of $-9.5 \text{ km}^2 \cdot \text{a}^{-1}$. The average annual ET is closely related to land-use types and shows a significant downward trend in general. The corresponding ET magnitude is exhibited as follows: forests>grasslands>croplands>wetlands>water bodies>urban/build-up lands>barren. Results of the study also suggest water conditions (precipitation (Pre) and relative humidity (RH) decrease) are major controlling factors in the decline of ET. Overall, the LUCC has a smaller influence on ET than climate change in the HRB. This research will provide a better insight into climate change and LUCC impacts on water resources.

Keywords Huai River Basin · Evapotranspiration · Climate change · Land use and land cover · MODIS

Responsible Editor: Philippe Garrigues

✉ Ronghao Chu
ronghao_chu@163.com

✉ Abu Reza Md. Towfiqul Islam
towfiq_dm@brur.ac.bd

¹ School of Resources and Environment, Anhui Agricultural University, Hefei 230036, China

² Hefei Scientific Observing and Experimental Station of Agro-Environment, Ministry of Agriculture, Hefei 230036, China

³ Anhui Public Meteorological Service Center, Anhui Meteorological Bureau, Hefei 230031, China

⁴ Department of Disaster Management, Begum Rokeya University, Rangpur 5400, Bangladesh

⁵ Key Laboratory of Meteorological Disaster, Ministry of Education (KLME), Joint International Research Laboratory of Climate and Environment Change (ILCEC), Collaborative Innovation Center on Forecast and Evaluation of Meteorological Disasters (CIC-FEMD), Jiangsu Key Laboratory of Agricultural Meteorology, College of Applied Meteorology, Nanjing University of Information Science & Technology, Nanjing 210044, China

Introduction

Huai River Basin (HRB), located in a typical climatic transition zone between north and south of China, is a commodity grain production base in China. In recent years, due to human impact and climate change, remarkable changes have occurred in the water cycle process, which has also brought critical challenge for water resources, ecological environment, and economic and social development. Evapotranspiration (ET), as an important climatic parameter, plays a pivotal role in surface water balance and the hydrological cycle (Chu et al. 2017). Therefore, studying change in surface ET characteristics, as well as its response to climate change and land use and land cover (LUCC), can provide a crucial theoretical basis for realizing the optimal allocation and sustainable development of regional water resources.

Previous studies on the actual ET were mainly based on the data from meteorological stations, without taking into account the surface vegetation cover and underlying surface type. When interpolating with the site ET to obtain regional ET, large errors may occur due to variations in surface type. Meanwhile, although the predecessors had adopted the data of meteorological stations as much as possible, the problem of sparse stations still exists. In recent years, the development of satellite remote sensing technology and related inversion algorithms made it possible to monitor surface vegetation cover and underlying surface type, offering continuous ET value on a large scale. Therefore, it is reasonable to use remote sensing product data to explore the impact of land-use type change on surface ET. In the past few decades, more and more models had used remote sensing data to estimate ET, including TSEB model (Norman et al. 1995), SEBAL model (Bastiaanssen et al. 1998a; Bastiaanssen et al. 1998b), S-SEBI model (Roerink et al. 2000), SEBS model (Su 2002), STSEB model (Sánchez et al. 2008), GLEAM model (Miralles et al. 2011), and MODIS-ET (Mu et al. 2011). The performance of the above models is convincible. Among them, based on Penman-Monteith equation and the land surface characteristics obtained by remote sensing data, the National Aeronautics and Space Administration (NASA) developed the global land evapotranspiration data product—MOD16, which had been verified by the global flux observation data, and the estimated accuracy was 86% (Gowda et al. 2008). Based on the high estimation accuracy and the accessibility of MOD16 data, this product has been widely used in the study of spatiotemporal variation characteristics of ET worldwide. Therefore, this study adopted the MOD16 and MCD12Q1 from the MODIS product datasets from 2001 to 2014 in the HRB.

At present, a number of studies have been performed on the influence of climate change on the ET in the HRB (Chu et al. 2017; Zou et al. 2017). In addition to the impact of climate

change, however, the land-use change caused by human activities is also one of the most important factors affecting the surface ET. Because different land-use types are characterized with different vegetation types, leaf area index (or vegetation coverage), and surface albedo (or surface optical characteristics), etc., when land-use types change, their corresponding ET capacity will change accordingly. Land-use type change has different impacts on surface ET in various basins of China. For example, deforestation may decrease ET (Olchev et al. 2008), and croplands offer much greater actual ET than built-up area (Liu et al. 2010). China experienced a rapid transformation of LUCC process in the twentieth century. Since most of the forested land was transferred to paddy or irrigated fields, deforestation reduced ET by an average of 422 mm·a⁻¹. Currently, changes in land-use patterns such as vegetation change (deforestation, afforestation or grassland reclamation), agricultural development activities (farmland reclamation, crop cultivation and agricultural management), and urbanization have seriously affected the regional ET, resulting in the intensified flood (Brath et al. 2006) and great changes in the base flow (Wang et al. 2006) and the annual average flow (Costa et al. 2003).

Furthermore, the ET rate of the HRB also varies with different land cover types on different underlying surfaces. At present, there are many studies on surface ET and land use in China, including Poyang Lake Basin (Wu et al. 2013), Sanjiang Plain (Feng et al. 2015), Shaanxi (Fan et al. 2014; Wang et al. 2016) and Anhui (Wang et al. 2018) provinces, Huan River Basin (Zhang et al. 2018b), and northwest China (Deng et al. 2017). However, the influence of land-use change on surface ET in the HRB is unclear. In water-scarce conditions, land-use transitions sometimes lead to enhanced competition for water (Feng et al. 2016). Current insights into the impacts of these competing requirements are yet inadequate (Menz et al. 2013). Particularly, the question of whether the land-use types have controlled surface ET trends or whether the impact of the meteorological factor on surface ET is outweighed by the impact of land-use types on surface ET remains undetermined.

Nevertheless, little is understood about changes in actual ET for diverse land-use types in the HRB. In this study, we hypothesized that the impacts of meteorological factors are much higher than that of the effects of land-use types that affecting surface ET. We tested the hypothesis by estimating transitions from different land-use types affecting surface ET. This study seeks to find the gaps in understanding of the role of climate change and LUCC on ET of the HRB. The prime objectives of the current study were (i) to investigate the spatiotemporal variation trends and characteristics of ET based on the Theil-Sen's trend estimation method and Mann-Kendall (MK) test, (ii) to analyze the actual surface ET change characteristics of different land-use types in the HRB, (iii) to clarify the correlation between ET and meteorological factors, and

(iv) to quantify the effects of climate change and LUCC on ET. This research will play an important role in effective planning, sustainable water resources management, and mitigating probable impacts of climate on the HRB water balance.

Study area and data

Study area

Huai River originates from Tongbai mountains in Henan province, which flows through Henan, Hubei, Anhui, and Jiangsu provinces from west to east. HRB locates between the Yangtze River Basin and the Yellow River Basin and belongs to the climate transition zone between north and south China (111° 55'~121° 25' E, 30° 55'~36° 36' N), which is considered to be the dividing line between China's warm temperate zone and the north subtropical zone (zero isotherms). The HRB has four distinct seasons and a mild climate. The HRB covers an area of about 270,000 km², and the length of its mainstream is about 1,000 km, with a total drop height of about 200 m. The western, southwestern, and northeastern areas of the HRB are mainly mountains and hills. The rest of the areas are vast plains, accounting for about two-thirds of the total area (Fig. 1). The HRB is divided into two major water systems, namely the Huai river system and Yi-Shu-Si river system, in which the Huai river system is subdivided into the upper, middle, and lower reaches (He et al. 2015). The average annual temperature increases from north to south and from coastal areas to inland, with an overall range of 11~16 °C. The average annual evaporation of water is between 900 and 1500 mm, the relative humidity is between

40 and 70%, and the average annual precipitation is about 970 mm, with more than 50% of the precipitation concentrated in the monsoon season from June to September. Due to the uneven distribution of precipitation and complicated weather system, the HRB is vulnerable to flood in the rainy season and drought in the dry season. In addition, because the study area is adjacent to the Yangtze River Delta (YRD) and Huang-Huai-Hai (HHH) plain, the population density of the HRB is about fivefold of the national average. The HRB is also the main grain production base of eastern China (Yan et al. 2010). The main crops include wheat, rice, maize, potato, rapeseed, soybean, and cotton, with output accounting for about 17.3% of the total national production. Shouxian National Climate Observatory (116° 46' E, 32° 33' N) is located on the south shore of the middle HRB, which represents a typical farmland ecosystem in the HRB. The cropping system is mainly rice-wheat crop rotation (Tian et al. 2011).

Data

Digital elevation model (DEM) data

The spatial resolution of the digital elevation model (DEM) employed in this research (Fig. 1) is 90 m; the data source is from <http://srtm.csi.cgiar.org/>.

Remote sensing data

The spatial resolution of MOD16 product data adopted in this study is 1 km × 1 km, the temporal resolution includes 8 day, month, and year time scales. The datasets, including the evapotranspiration (ET), latent heat flux (LE), potential ET (PET), and potential LE (PLE), have been widely validated and used around the world (Mu et al. 2011). This research mainly adopts the synthetic product data of MOD16 in day, month (MOD16A2), and year (MOD16A3) timescales during 2001–2014; it can be downloaded from the website of the University of Montana Digital Earth Dynamic Simulation Research Group (<http://www.ntsg.umt.edu/project/mod16>). Based on the geographical location of the HRB and the line number distribution map from MODIS product in China, the remote sensing images covering the HRB were selected, the specific satellite orbit numbers are h27v05 and h28v05.

The land cover type data adopted in this study was MCD12Q1 product data of MODIS during 2001–2014, with a spatial resolution of 500 m × 500 m. This product used the International Geosphere-Biosphere Programme (IGBP) to classify the global surface types into 17 types. In this study, based on the main vegetation types of the HRB, the surface type was reclassified into 7 types, namely croplands, forests, grasslands, urban/built-up, water bodies, wetlands, and barren. The nearest neighbor resampling method was also adopted in this study to interpolate the MOD16 data with a

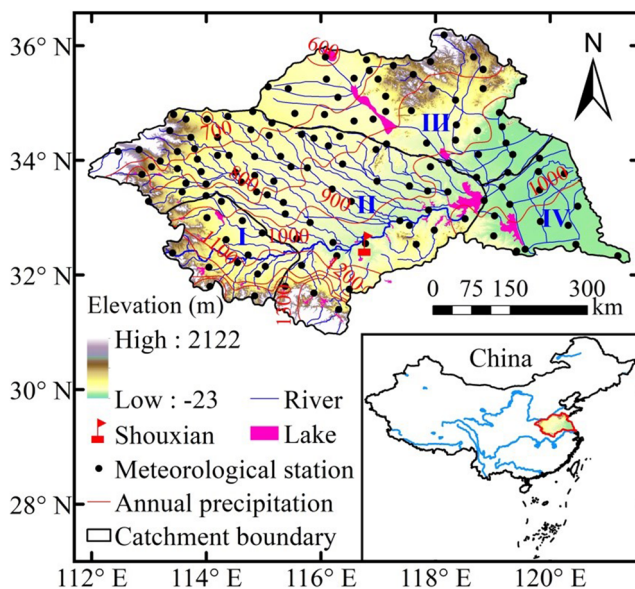


Fig. 1 Location of the Huai River Basin (HRB) in China. I: Upper HRB; II: Middle HRB; III: Yi-Shu-Si basin; IV: Lower HRB

resolution of 1 km × 1 km to the spatial resolution of 500 m × 500 m, to unify the accuracy of MOD16 ET and MCD12Q1 datasets. Due that the MODIS product data is based on the HDF format of SIN projection, the MODIS Reprojection Tool (MRT) was used to preprocess the original data in this study. Detailed data description can be found in the data user guide of the above data download website.

Hydrological, meteorological, and eddy covariance data

To verify the applicability of the MOD16 ET product data, the annual precipitation and runoff data of the HRB during 2001–2014 were selected in this study. The datasets were obtained from the Huai River Water Resources Bulletin (<http://www.hrc.gov.cn/>) issued by the Huai River Commission of the Ministry of Water Resources.

Furthermore, in order to explore the correlation mechanism between ET and meteorological factors, daily meteorological data of 137 meteorological stations from 2001 to 2014 released by the National Meteorological Information Center (NMIC) of the China Meteorological Administration (CMA) were employed in this study. This data sets included the mean temperature (T_a , °C), precipitation (Pre, mm), relative humidity (RH, %), wind speed at 10-m height (u_{10} , m·s⁻¹), and sunshine duration (SD, h). In addition, to further prove the validity of MOD16 product data, the D20 pan evaporation data (E_{pan} , mm) of 89 meteorological stations (Li et al. 2018b) during 2001 to 2013 were also adopted here to verify the MOD16 PET data. The eddy covariance (EC) measurements during 2008–2009 provided by the Shouxian National Climate Observatory were employed to verify the MOD16 monthly ET data, and the specific information of EC

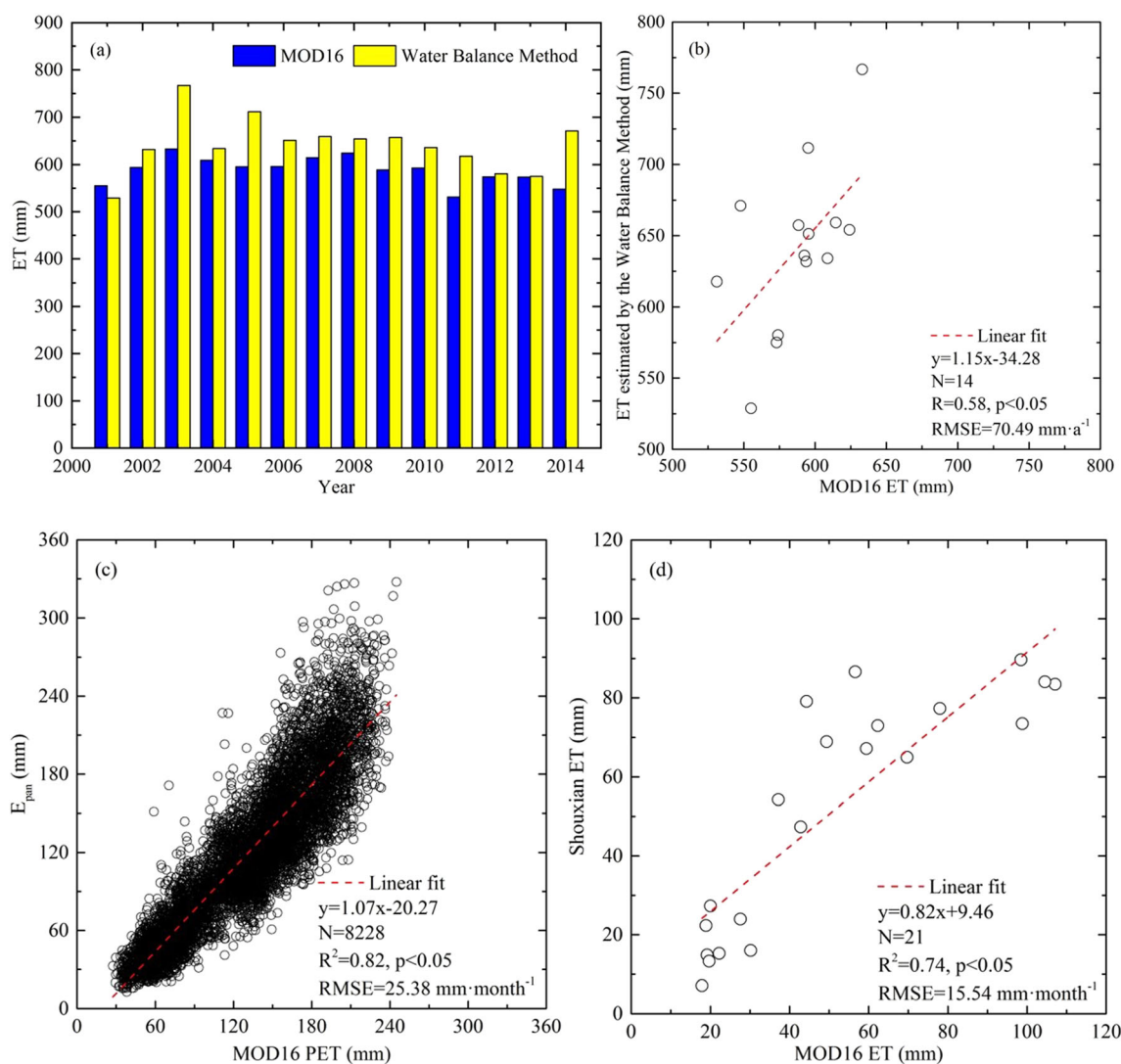


Fig. 2 Validation of the applicability of annual MOD16 ET product data using the water balance method (a, b), MOD16 PET product data using monthly E_{pan} data (c) during 2001–2013 and monthly MOD16 ET product data using EC measurements by Shouxian flux tower during rice-

wheat growing seasons in 2008 and 2009 (d). Note: The monthly EC measurements were from November 2007 to September 2009, except June and October in 2008

measurements could be found in the literature referenced in Chu et al. (2019) and Li et al. (2020).

Quality control of the meteorological data sets had already been carried out by the staff members of the NMIC. Detailed data descriptions can be checked from the website <http://data.cma.cn/>. Conversion formula of u_{10} to wind speed at 2 m (u_2) and SD to net radiation (R_n) can be referred to Li et al. (2018a).

Methods

Water balance method

In this study, the water balance method was adopted to verify the applicability of MOD16 ET product data. The specific calculation formula is as follows:

$$ET_a = Pre - R - \Delta S \tag{1}$$

where ET_a represents the actual surface evapotranspiration (mm), Pre represents the precipitation (mm), R represents the surface runoff (mm), and ΔS refers to the net changes in surface and underground water storage (mm). Due to the effects of natural and human factors, ΔS are difficult to determine and can be ignored on a yearly or multi-year time scale.

Trend analysis

In this research, Theil–Sen’s slope estimator (Sen 1968; Theil 1950) was used to estimate the magnitude of the variables’ trends. In addition, the nonparametric Mann–Kendall (M-K) test (Mann 1945), which has been widely used in hydrological trend detection studies, was also applied to determine the significance of the variables’ trends. Detailed descriptions of these methods can be found in Li et al. (2018b).

Assessment of the impact of climate change and LUCC on ET

To quantify the influence of climate change and LUCC on ET, we followed the approach by Odongo et al. (2019) and introduced the concept of ET volume from climate change and LUCC; specific calculation processes are as follows:

$$Vol_{t_i}^{LUCC} = \sum (ET_{t_i}^{LUCC} - ET_{t_{i-1}}^{LUCC}) \times \text{pixel area} \tag{2}$$

$$Vol_{t_i}^{Climate} = \sum (ET_{t_i}^{Climate} - ET_{t_{i-1}}^{Climate}) \times \text{pixel area} \tag{3}$$

where $Vol_{t_i}^{LUCC}$ is the volume of total water from LUCC for the current year t_i and $ET_{t_i}^{LUCC}$ and $ET_{t_{i-1}}^{LUCC}$ are the ET for changed land-use type of each pixel for the current year t_i and previous year t_{i-1} , respectively. The pixel area is the actual area of single pixel, which is 250000 m².

where $Vol_{t_i}^{Climate}$ is the volume of total water from climate change for the current year t_i , and $ET_{t_i}^{Climate}$ and $ET_{t_{i-1}}^{Climate}$ are the ET for unchanged land-use type of each pixel for the current year t_i and previous year t_{i-1} , respectively. The pixel area is the actual area of single pixel, which is also 250000 m².

Results

Applicability verification of MOD16 product data

Prior to using MOD16 products to estimate the actual ET in the HRB, the accuracy and validity of MOD16 are needed to be verified for the present study. Thus, the annual ET estimated from annual precipitation and runoff data by the water balance method (Eq. 1) was compared with the MOD16 ET data (Fig. 2a, b). From Fig. 2a, the overall error between the annual ET estimated by the water balance method and the MOD16 ET was relatively small, and the MOD16 ET was generally underestimated. In addition, the scatter fitting graph (Fig. 2b) showed that the two ET were in good agreement with each other, with a root-mean-square error (RMSE) of 70.49 mm·a⁻¹, a correlation coefficient (R) of 0.58, and a significant correlation ($p < 0.05$). This indicated a reasonable accuracy of MOD16 ET data in this research. In order to further verify the validity of the MOD16 product data, we also adopted the monthly E_{pan} data during 2001–2013 to validate the MOD16 PET data and EC measurements by Shouxian flux tower during rice–wheat growing seasons in 2008 and 2009 to validate the monthly MOD16 ET product data here. As shown in Fig. 2c, we can find there was a significant linear relationship ($p < 0.05$) between E_{pan} and MOD16 PET, with the R square value (R^2) of 0.82 and RMSE of 25.38 mm·month⁻¹.

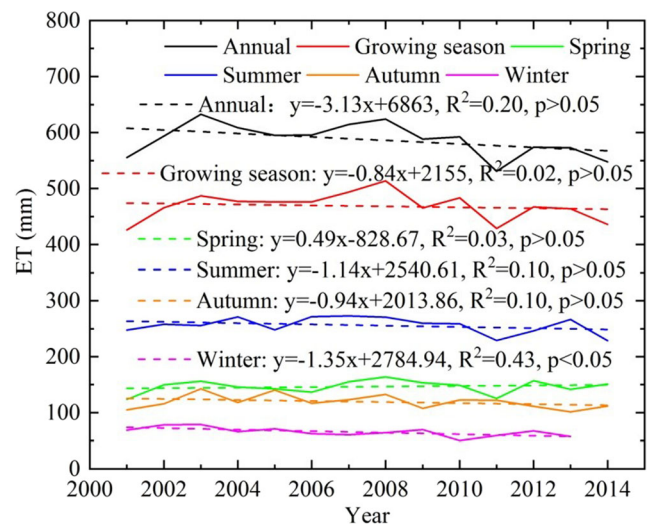


Fig. 3 Temporal variation characteristics of ET in the HRB during 2001–2014

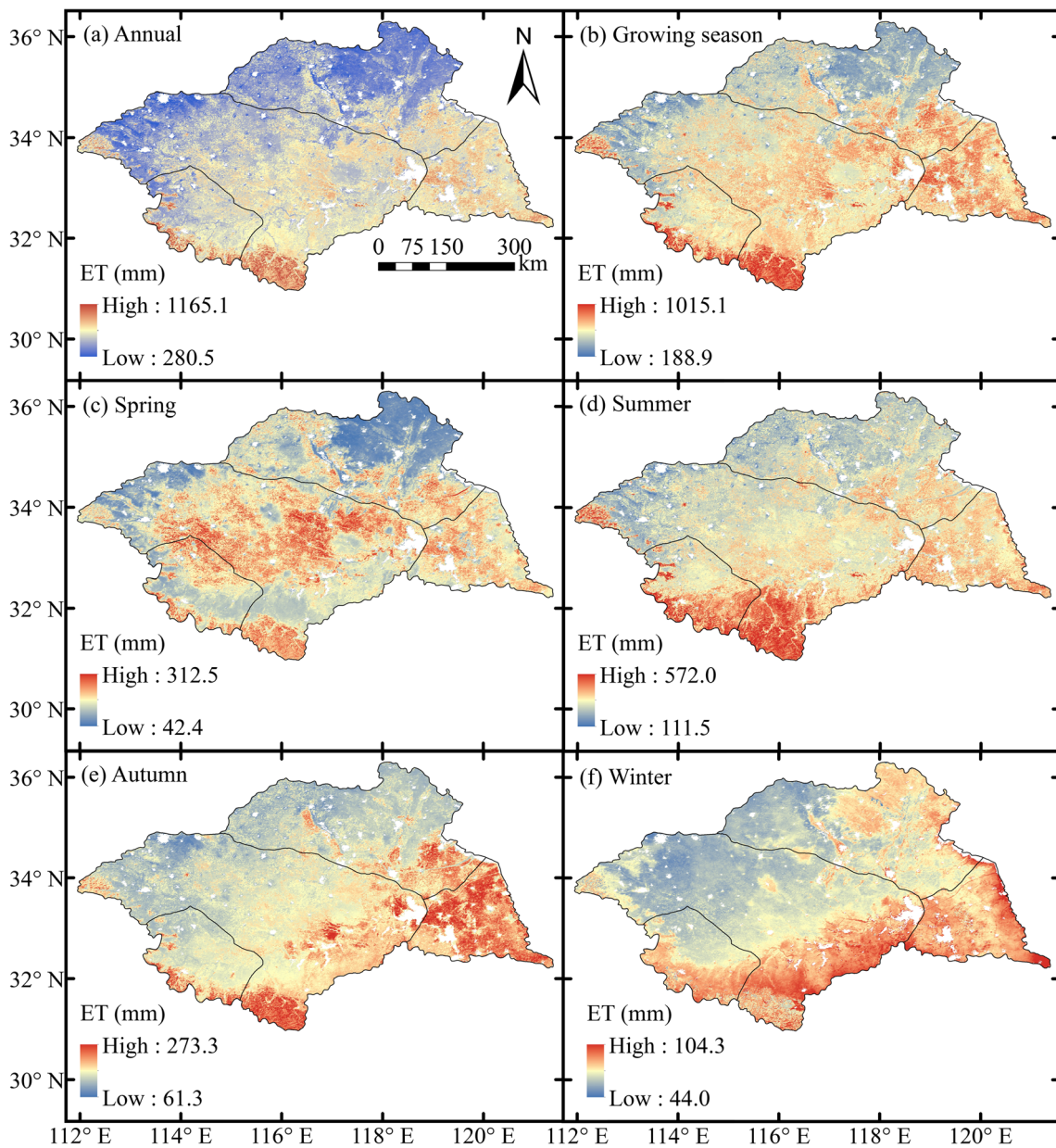


Fig. 4 Spatial distribution of ET in the HRB during 2001–2014

Moreover, a significant linear relationship ($p < 0.05$) between Shouxian ET and MOD16 ET was also shown in Fig. 2d, with R^2 of 0.74 and RMSE of $15.54 \text{ mm} \cdot \text{month}^{-1}$. Thus, all these phenomena verified that the accuracy of MOD16 product data was adequate and could be used to estimate the ET in the HRB.

Spatiotemporal variation characteristics of ET during 2001–2014

From Fig. 3, it can be seen that except for spring ($0.49 \text{ mm} \cdot \text{a}^{-1}$), the ET in the annual, growing season, summer, autumn, and winter present decreasing trends, with a rate of $-3.13 \text{ mm} \cdot \text{a}^{-1}$.

Table 1 Statistical significance test of ET change trend in the HRB (percentage of total area)

ET trend	Annual	Growing season	Spring	Summer	Autumn	Winter
Decreasing (S)	24.71%	11.75%	12.16%	14.09%	14.09%	53.32%
Decreasing (NS)	51.07%	45.84%	34.86%	53.58%	61.39%	43.63%
Increasing (S)	1.99%	5.16%	16.92%	2.44%	2.59%	0.01%
Increasing (NS)	22.23%	37.26%	36.06%	29.89%	21.93%	3.04%

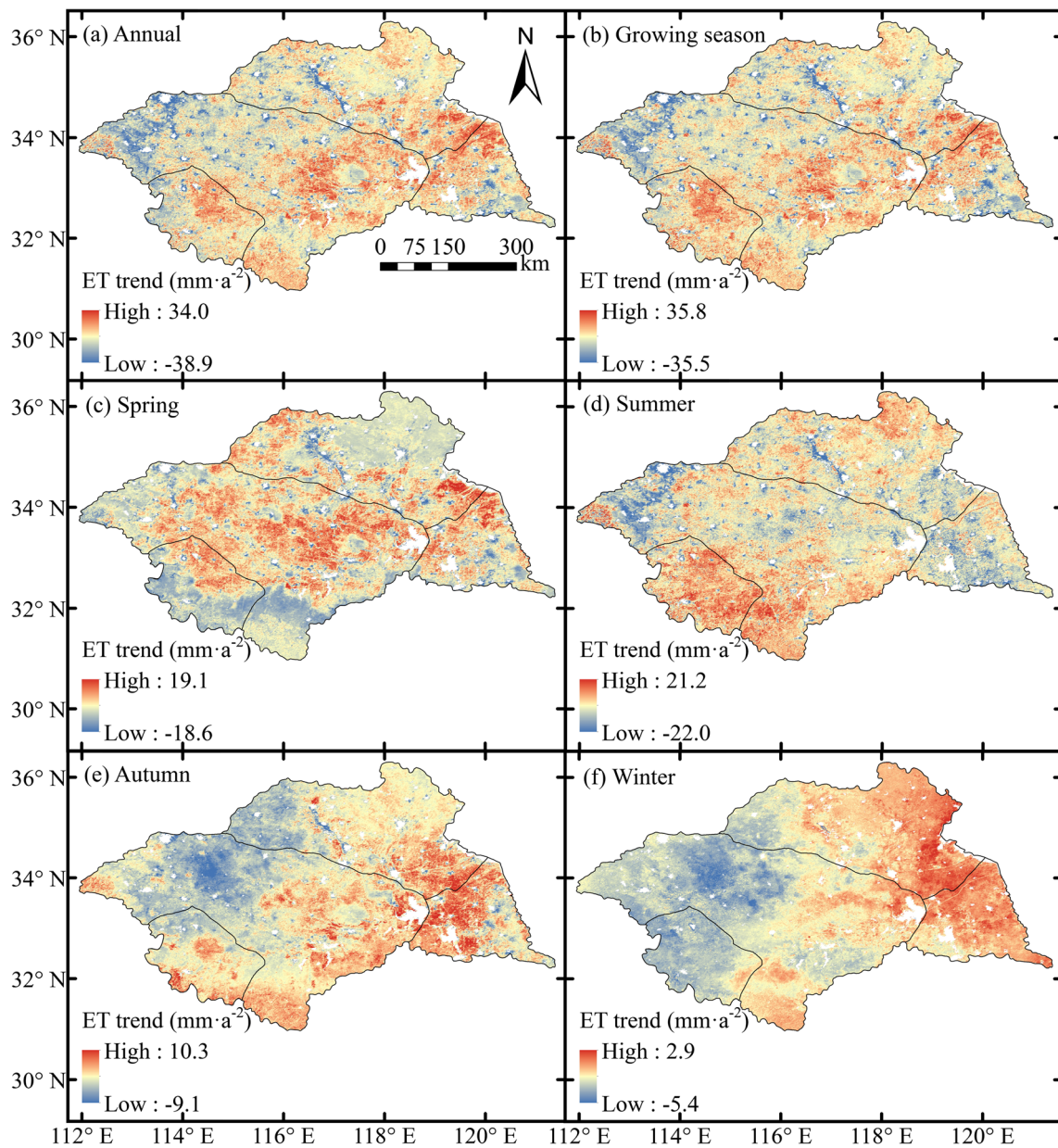


Fig. 5 Spatial distribution of ET trends in the HRB during 2001–2014

a^{-1} , $-0.84 \text{ mm}\cdot\text{a}^{-1}$, $-1.14 \text{ mm}\cdot\text{a}^{-1}$, $-0.94 \text{ mm}\cdot\text{a}^{-1}$, and $-1.35 \text{ mm}\cdot\text{a}^{-1}$, respectively. The significance is found from the ET in winter ($p < 0.05$).

As shown in Fig. 4, the average annual ET in the HRB ranges from 280.5 to 1165.1 mm, the higher value distributes in the south and lower values in the north. The high-value area in the southwest is also with a high altitude. The distribution of ET in the growing season and summer are consistent with the annual. The values are between 188.9 and 1051.1 mm for the growing season and 111.5 and 572 mm for summer. The high-value area in the southwest expands in the summer season. The distribution pattern of ET (42.4–312.5 mm) in spring differs from that in annual and growing seasons, and the high-value area is mainly

concentrated in the middle area. The high ET values in autumn are mostly identified in the southwest of the middle HRB and the lower HRB. The ET is the lowest in winter, ranging from 44.0 to 104.3 mm. The high-value area is mainly distributed in the south HRB and most of the Yi-Shu-Si river basin. Meanwhile, ET distribution is divided by the Huai River, and ET is lower in the north of the Huai River and higher in the south.

Figures 5 and 6 and Table 1 together indicate that the annual ET variation trend of the HRB is between -38.9 and $34.0 \text{ mm}\cdot\text{a}^{-2}$, with about 75.78% of the area showing a decreasing trend, and the area with a significant decreasing trend accounting for about 24.71% of the total area, which mainly distributes in the northwest of the middle HRB and the southeast of

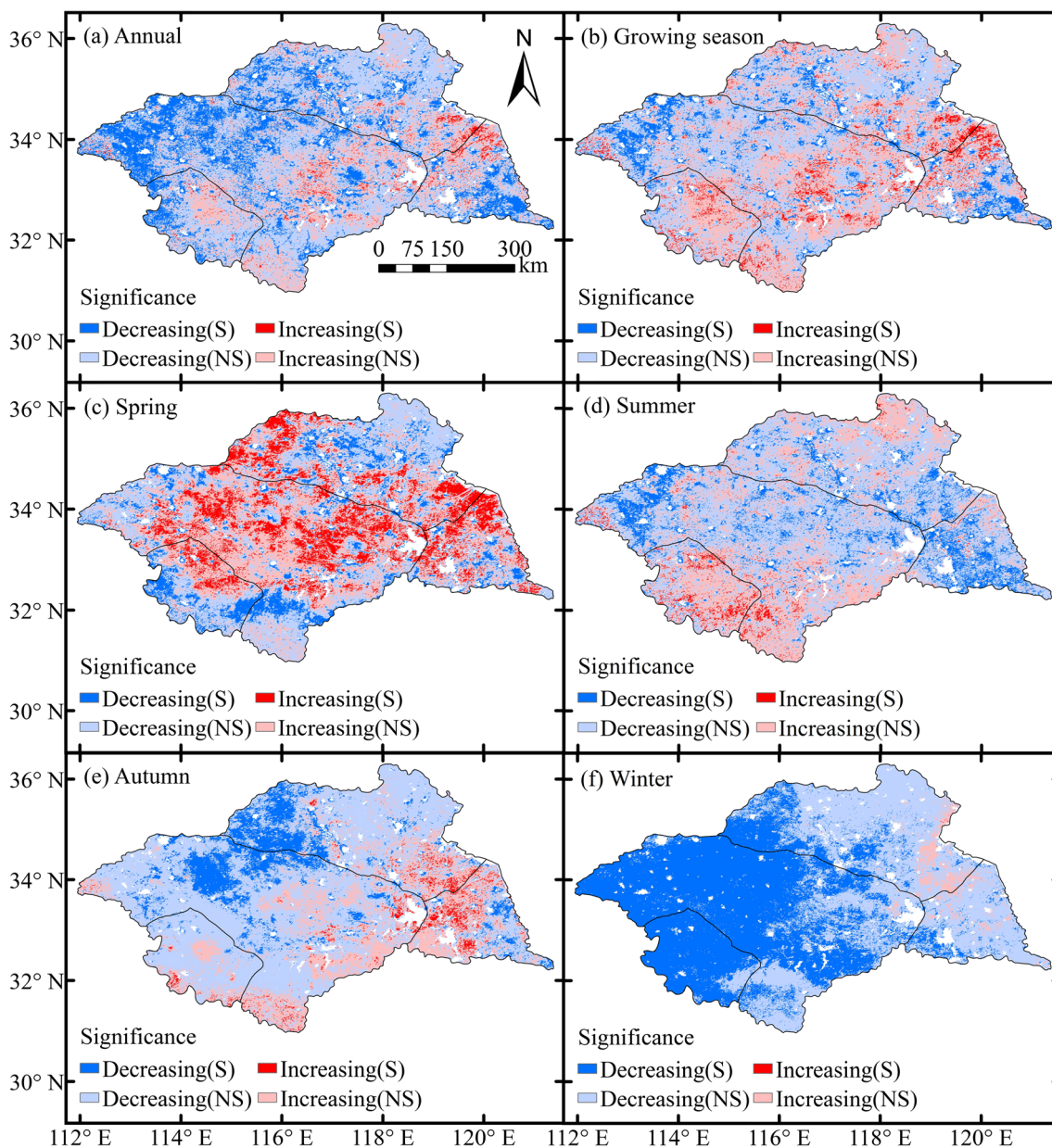


Fig. 6 Spatial distribution of ET trend significance in the HRB from 2001 to 2014

the lower HRB. However, ET shows an increased trend in the middle and eastern parts of the HRB, and only 1.99% of the areas shows significance. The significant changing trend of ET in the growing season is similar to that in the annual time scale. In spring, more area shows an increasing ET trend, accounting for about 52.98% of the total area, in which the significantly increasing ET area proportion is 16.92%, mainly distributed in the central part of the middle HRB, the northern part of the lower HRB, and the northwestern part of the Yi-Shu-Si river basin. In summer, ET shows a general declining trend, which is similar to that in the annual time scale and growing season. Meanwhile, about 67.67% area exhibits a declining trend, of which about 14.09% shows the

significance, mainly located in the northwest of the middle HRB and some part of the lower HRB. The area with significant increasing ET trend is mainly located in the southwest of the HRB. In autumn, about 75.48% area shows decreasing ET trend, mainly located in the northwest of the HRB. The area with a significant decreasing ET trend is mainly located in the central and northern parts of the HRB, accounting for about 14.09% of the total area. The changing trend of ET in winter is different from that of other seasons. About 96.95% area expresses decreasing ET trend, of which 53.32% of the total area shows a significant decreasing trend, mainly located in the upper and middle HRB and the northwest part of lower HRB and Yi-Shu-Si river basin.

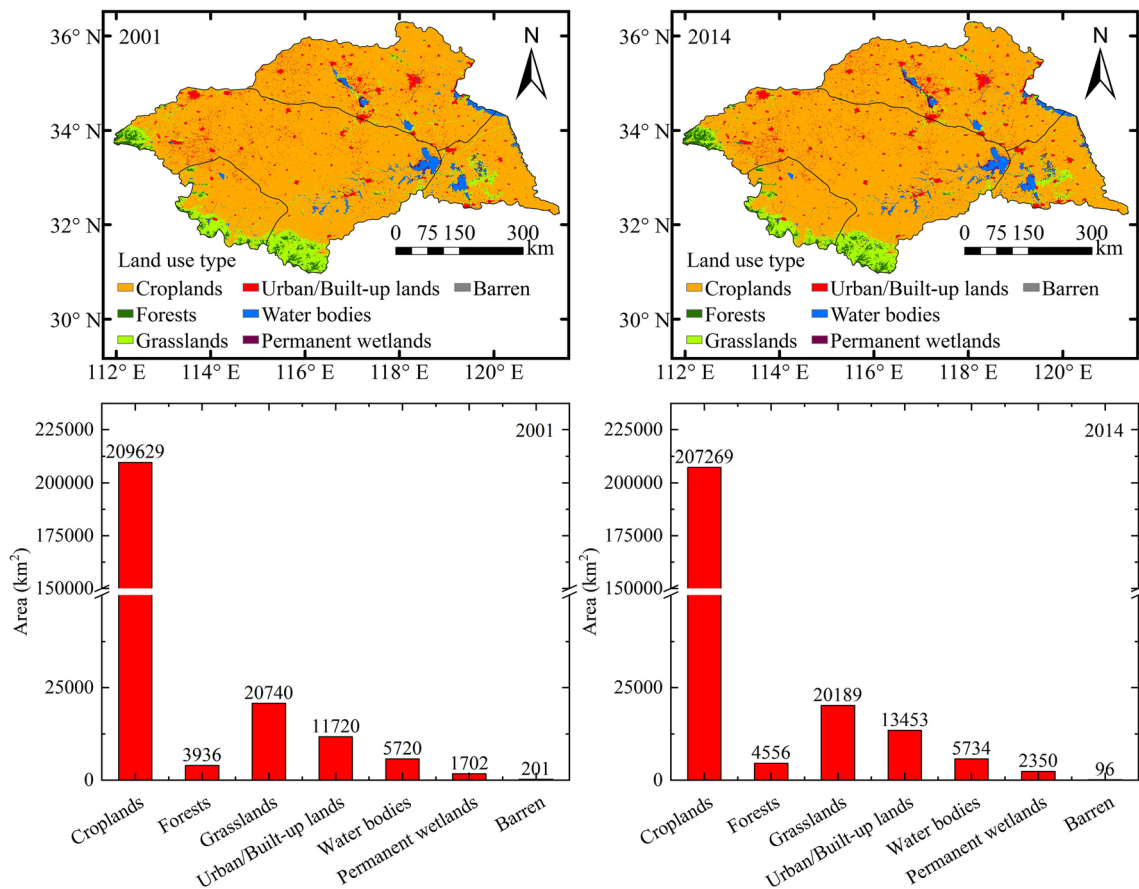


Fig. 7 Land cover type map of HRB after reclassification in 2001 and 2014

Analysis of land-use change

As shown in Fig. 7, the distribution map of land cover types after reclassification in the HRB between 2001 and 2014 was selected here. It can be seen that the land-use type in the HRB is mainly croplands, the areas with higher elevations in southwest and northwest HRB are forests and grasslands, and some areas in the lower HRB are also covered by grasslands. The overall land-use type area is displayed in order: croplands>grasslands>urban/built-up>water bodies>forests>permanent wetlands>barren. In order to more intuitively understand the changing trend of land cover types in the HRB during the past 14 years, ArcGIS was employed to extract the annual area of each land-use type. As shown in Fig. 8, the croplands area in the HRB showed a decreasing trend at a rate of $-176.2 \text{ km}^2 \cdot \text{a}^{-1}$, with the R^2 value of 0.92. Before 2010, the area of forests showed a gradually increasing trend, but showed a decreasing trend after 2010, with an overall increased rate of $40.9 \text{ km}^2 \cdot \text{a}^{-1}$. The grasslands decreased significantly from 2001 to 2004, increased slowly from 2004 to 2007, decreased from 2007 to 2010, and increased again after 2010. The grasslands area presents a w-type fluctuation decreasing trend, with an overall rate of $-35.8 \text{ km}^2 \cdot \text{a}^{-1}$. The urban/built-up area increased at a rate of $138.3 \text{ km}^2 \cdot \text{a}^{-1}$, with

the R^2 value as high as 0.99. The water bodies area increased significantly before 2006 and then decreased significantly after 2006, and this trend slowed down after 2010, gradually decreasing at an overall rate of $-1.38 \text{ km}^2 \cdot \text{a}^{-1}$. The wetlands area increased significantly at a rate of $43.6 \text{ km}^2 \cdot \text{a}^{-1}$, with an R^2 value as high as 0.94. The wetlands area increased rapidly before 2004, and then, the increasing rate was slower than before. Over the past 14 years, the barren area gradually decreased at a rate of $-9.5 \text{ km}^2 \cdot \text{a}^{-1}$, and the R^2 value was as high as 0.94. However, the decline rate slowed down after 2012.

Table 2 shows the transfer matrix of land-use type for the HRB from 2001 to 2014. It can be seen that, during the past 14 years, although there are 3962.5 km^2 grasslands converted into croplands, the overall croplands area decreased by 2360 km^2 , and the area size of croplands transformed into other land cover types was in the following order: grasslands>urban/built-up>permanent wetlands>forests>barren, predominantly grasslands and urban/built-up. Due to a large area of grasslands (972.5 km^2) converted into forests, the forests area eventually increased by 620.5 km^2 , while the area converted into grasslands was small, only 389.5 km^2 . The grassland area decreased by 551.25 km^2 on the whole, and the area size converted to other land cover types was in order: croplands>forests>permanent wetlands>urban/built-

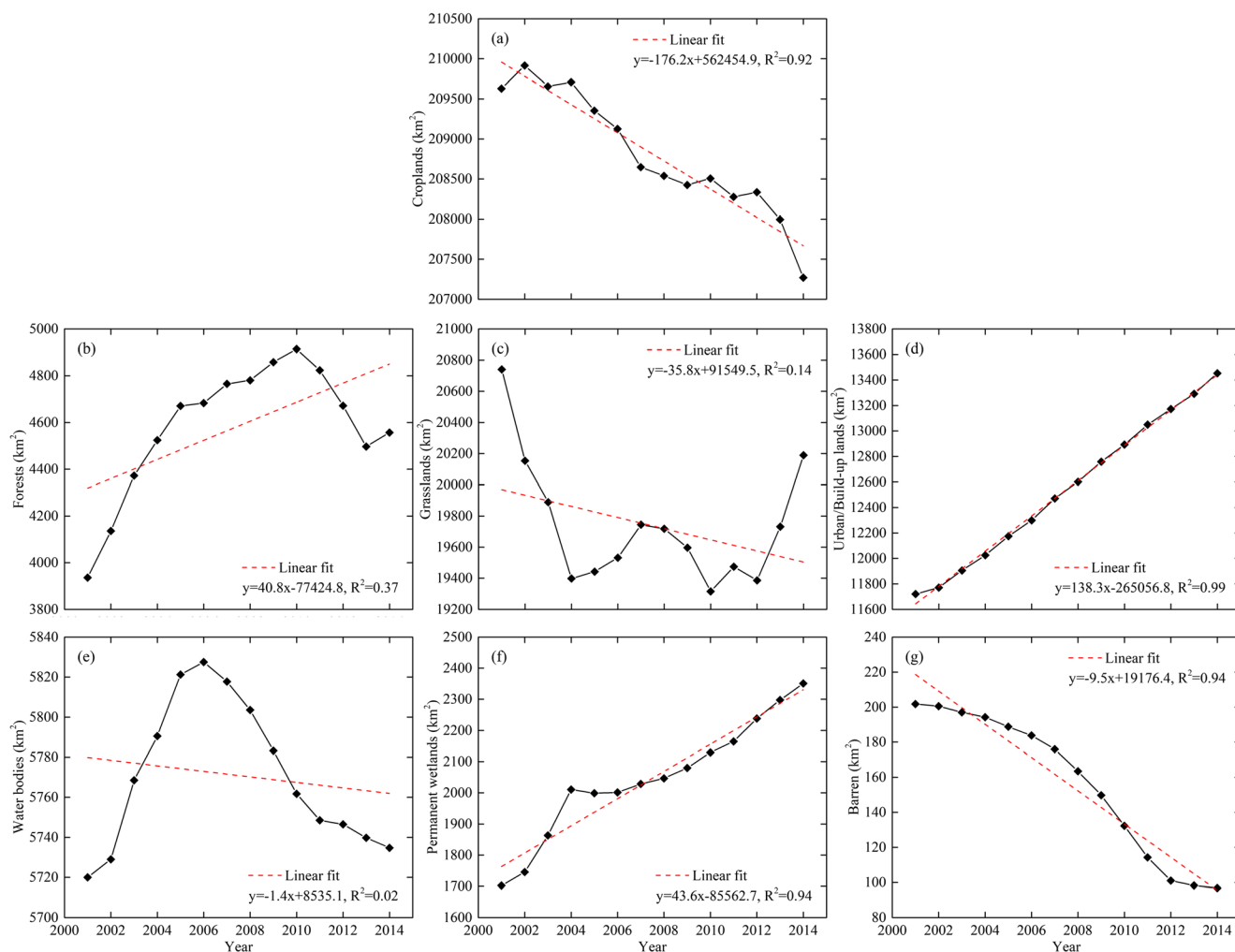


Fig. 8 Change trends of different land cover type areas in the HRB from 2001 to 2014

up>barren>water bodies. The overall urban/built-up area increased by 1733 km², which was mainly converted from croplands and grasslands, while the main urban area had no transformation. The overall water bodies area increased by 4.75 km², which was mainly converted into wetlands (16.5 km²),

and the land types converted into water bodies were mainly wetlands and barren. The wetlands area increased by 648.25 km² in total, and the main land types converted into wetlands were in the following order: grasslands>croplands>barren>water bodies, while wetlands were mainly converted

Table 2 Transfer matrix of land-use types in the HRB from 2001 to 2014 (km²)

	2014							
2001	Croplands	Forests	Grasslands	Urban/Built-up	Water bodies	Permanent wetlands	Barren	Total area
Croplands	<i>203238.5</i>	48.25	4813.25	1376	2	143.5	7.75	209629.3
Forests	12.75	<i>3534</i>	389.5	0	0	0	0	3936.25
Grasslands	3962.5	972.5	<i>14721.5</i>	327.25	1.5	743.5	12	20740.75
Urban/Built-up	0	0	0	<i>11720.5</i>	0	0	0	11720.5
Water bodies	0	0	0.75	0.25	<i>5701.25</i>	16.5	1.25	5720
Permanent wetlands	49	2	245	12.25	22.25	<i>1368</i>	4	1702.5
Barren	6.5	0	19.25	17.25	7.75	79.25	<i>71.75</i>	201.75
Total area	207269.3	4556.75	20189.25	13453.5	5734.75	2350.75	96.75	253651

Note: The numbers in italics on the diagonal show the land cover area that remained the same type between 2001 and 2014.

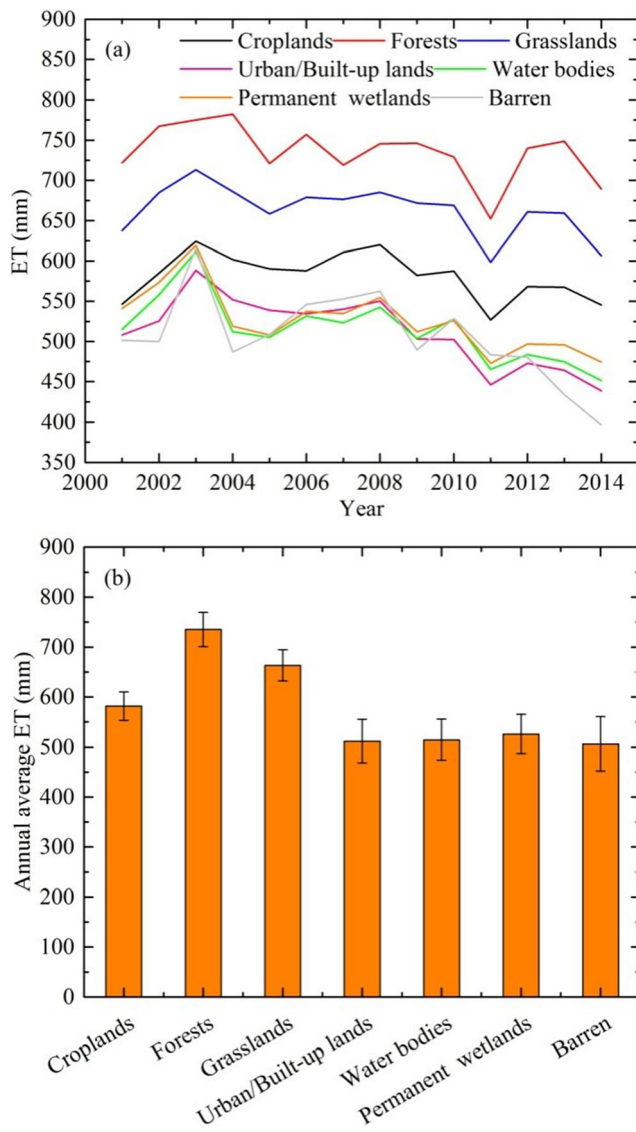


Fig. 9 ET variation trends of different land cover types in the HRB from 2001 to 2014

into grasslands. The total area of barren land decreased by 105 km², mainly converted from grasslands and croplands, and converted into wetlands, grasslands and urban/built-up.

Variation characteristics of ET of different land-use types

Different land-use types have different ET rates due to their physiological and ecological characteristics and precipitation conditions. As shown in Fig. 9, this study adopts the spatial statistics function of ArcGIS to extract the annual ET corresponding to the regional scale of each land-use type year by year. As can be seen from the figure, the annual ET is closely related to the land-use types of the HRB, and there is a profound difference between land-use types. In the past 14 years,

the ET of each land-use type all showed a significant declining trend. The average annual ET of forests land was the highest, with the value up to 735.3 mm·a⁻¹, followed by grasslands and croplands, where the average annual ET was 663.3 mm·a⁻¹ and 581.7 mm·a⁻¹, respectively. However, the annual ET and its variation trend in urban/built-up, water bodies, wetlands, and barren are relatively small. The annual ET is in the following order: wetlands (526.1 mm·a⁻¹)>water bodies (514.8 mm·a⁻¹)>urban/built-up (511.8 mm·a⁻¹)>barren (506.2 mm·a⁻¹).

Correlation mechanism between ET and meteorological factors

As shown in Fig. 10, the Pre exhibited a non-significant decreasing trend in the HRB for the past 14 years, with a rate of -9.26 mm·a⁻¹. T_a showed no change trend. RH showed a significant decreasing trend, with a rate of -0.37a⁻¹. u₂ presented a significant decreasing trend, with a rate of -0.018 m·s⁻¹·a⁻¹. However, R_n exhibited a non-significant decreasing trend generally.

In order to explore the correlation relationship between ET and meteorological factors, we chose five meteorological factors (namely Pre, T_a, RH, u₂, and R_n) from 137 meteorological stations. Then, we carried on the analysis from the temporal and spatial scale. At temporal scale, we determined the spearman correlation coefficient between annual average ET and each meteorological factor (Fig. 11). As shown in Fig. 11, we could detect that only the Pre and RH significantly correlated with ET, both with significance level of 0.05 and R² value of 0.40 and 0.33, respectively. At spatial scale, we adopted ArcGIS to carry out spatial interpolation of each meteorological factor and generated raster layers with the same spatial resolution as MOD16 ET product data. Then, we calculated the correlation relationship between ET and each meteorological factor at pixel level to obtain the R² and p values of each pixel. Then, we extracted R² of the pixel in which the p value was less than 0.05 (Fig. 12). As shown in Fig. 12, the spatial correlation between ET and Pre, T_a, RH, u₂, and R_n were 0.28~0.95, 0.28~0.79, 0.28~0.92, 0.28~0.93, and 0.28~0.86, respectively. Similar with Fig. 11, from the extracted area of the region, the correlation between ET and climate factors was as follows: Pre>RH>u₂>R_n>T_a. Thus, in terms of meteorological factors, the ET in the HRB was dominated by the reduced Pre and RH generally.

Influence of climate change and LUCC on ET

To quantify the influence of climate change and LUCC on ET, we introduce the volume of total water released by climate change and LUCC, respectively. As shown in Fig. 13, the

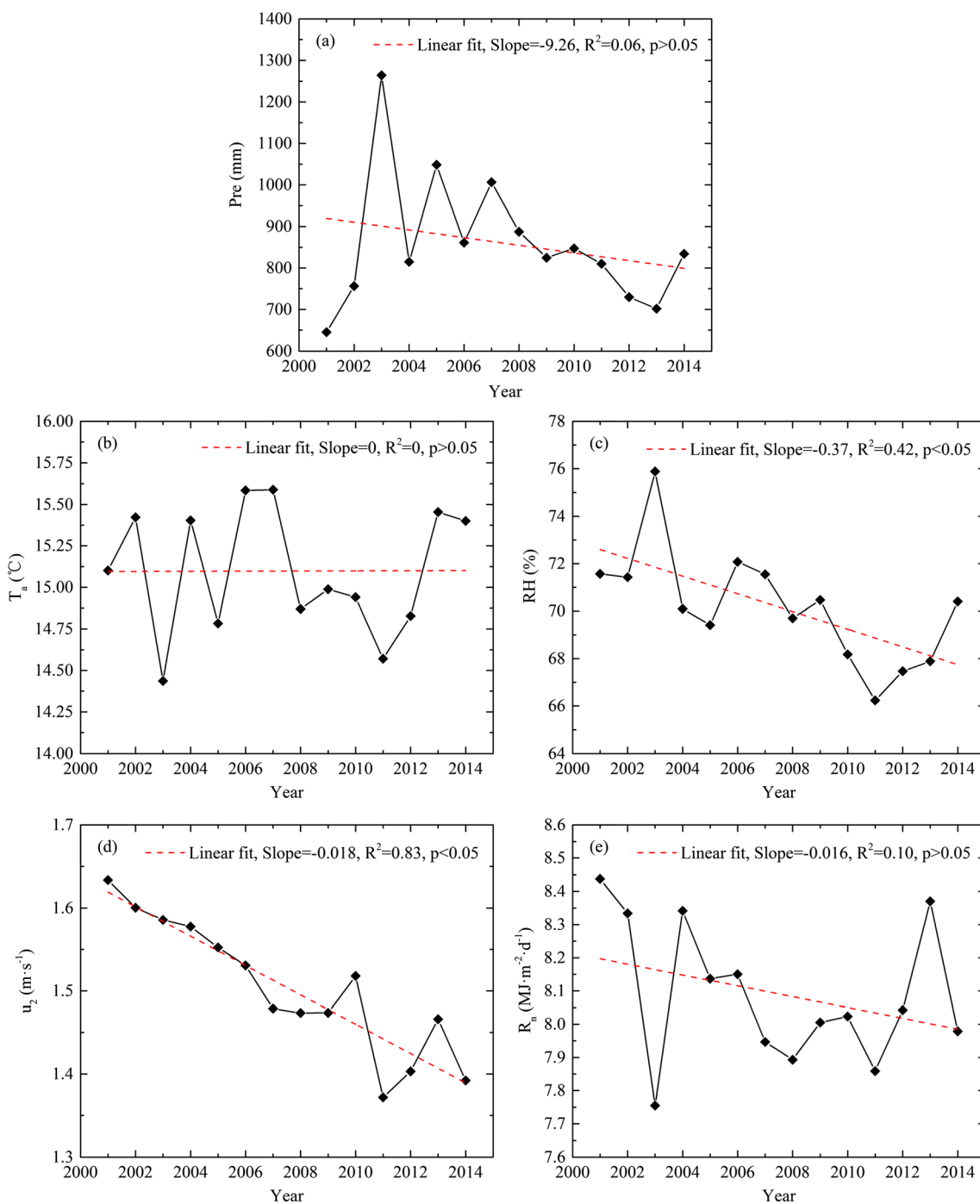


Fig. 10 Temporal variations of meteorological factors in the HRB during 2001-2014

change trend of ET contribution by volume from LUCC and climate change varied simultaneously (Fig. 13a), and the correlation coefficient is 0.90 (Fig. 13b). Moreover, the magnitude of ET contribution by volume from climate change ($10^9 \text{ m}^3 \cdot \text{a}^{-1}$) is larger than that from LUCC ($10^7 \text{ m}^3 \cdot \text{a}^{-1}$). Thus, the influence of climate change on ET is larger than LUCC in the HRB.

Discussion

Meteorological factors influencing ET

Meteorological factors are key factors that influence ET (Han et al. 2019; Vörösmarty et al. 2000; Vörösmarty and Sahagian 2000; Xu et al. 2015; Zou et al. 2017). It is generally

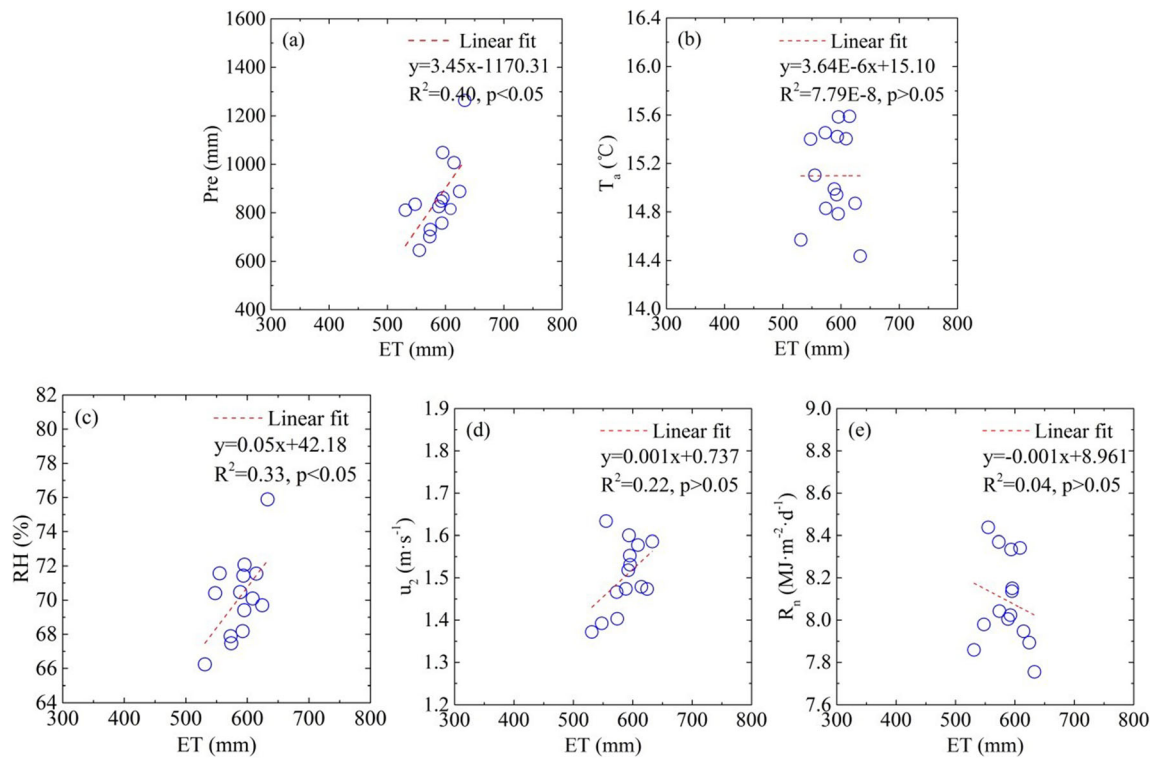


Fig. 11 The correlation between annual ET and corresponding meteorological factors at temporal scale. Note: **a**, **b**, **c**, **d** and **e** represent the Pre, T_a , RH, u_2 , and R_n , respectively.

acknowledged that water conditions, predominantly Pre and RH, are major drivers that control ET (Han et al. 2019; Lettenmaier and Famiglietti 2006; Shan et al. 2015). Our study also indicated that the decreasing Pre and RH are the main driving factors for the declining ET of the HRB in nearly 14 years. Similar results could also be found in the source region of the Yellow River (Ye et al. 2018), Haihe River Basin (Huang et al. 2019), and Dongting Lake Basin (Zhang et al. 2018a) of China, where the effects of Pre on ET are both stronger than those of T_a . Pre is one of the vital hydrologic parts of the water cycle, accounting for the water supply, further affecting ET to a certain degree (Walter et al. 2004). However, a reduction in Pre confirmed that there was low-moisture condition prevailing that suppressed surface ET over the 14 years. This is consistent with the findings of Jung et al. (2010), where ET declined due to low moisture supply in the southern Hemisphere rather than by changes in atmospheric conditions. The results of this study also showed that annual surface ET exhibited a decreasing trend in the 14-year period, which is similar with a prior study of ET in the HRB estimated by the Advection–Aridity model (Chu et al. 2019). Moreover, Chu et al. (2019) also demonstrated that RH was the dominant factor of actual ET trends in spring and was the second dominant factor in annual timescale during 1991–2014. The reduction of RH was related to the change in dry or wet surface conditions (Waring and Running 2007), thus affecting ET to some extent. The thermodynamic factors (increasing T_a and

decreasing R_n) and dynamic factor (reducing u_2) are generally related to raising amounts of cloudiness and aerosols in the atmosphere (Roderick et al. 2009; Stanhill and Cohen 2001), and also, rising surface albedo and surface temperature due to land-use changes may be contributed to the decrease in ET.

Land-use types influencing ET

Recently, plenty of studies have been conducted in China based on different land-use types (human activities) affecting ET (Feng et al. 2016; Liu and Hu 2019; Ma et al. 2019; Wang et al. 2019). In addition to meteorological factors, ET is more susceptible to land-use types (Gong et al. 2017; Han et al. 2019; Liu and Hu 2019). In addition, some researchers suggested that land-use types might have a more substantial effect on the water cycle than climate change (Boisier et al. 2014; Kundu et al. 2017; Zhao et al. 2017). Our study area covers the watershed land-use types, which mainly consisted of croplands. The impact of land-use types on regional ET is chiefly an outcome of physical variation in the land surface which influences the efficiency of ET (Dias et al. 2015; Douglas et al. 2009). Zhao et al. (2017) showed that the effect of human activities on ET is significantly larger than climate change. However, contrary to the prior study, our study reveals that land-use types have little influences on ET variations. Land transformation (Bronstert et al. 2002) alters properties such as temperature and soil moisture and further alters the water

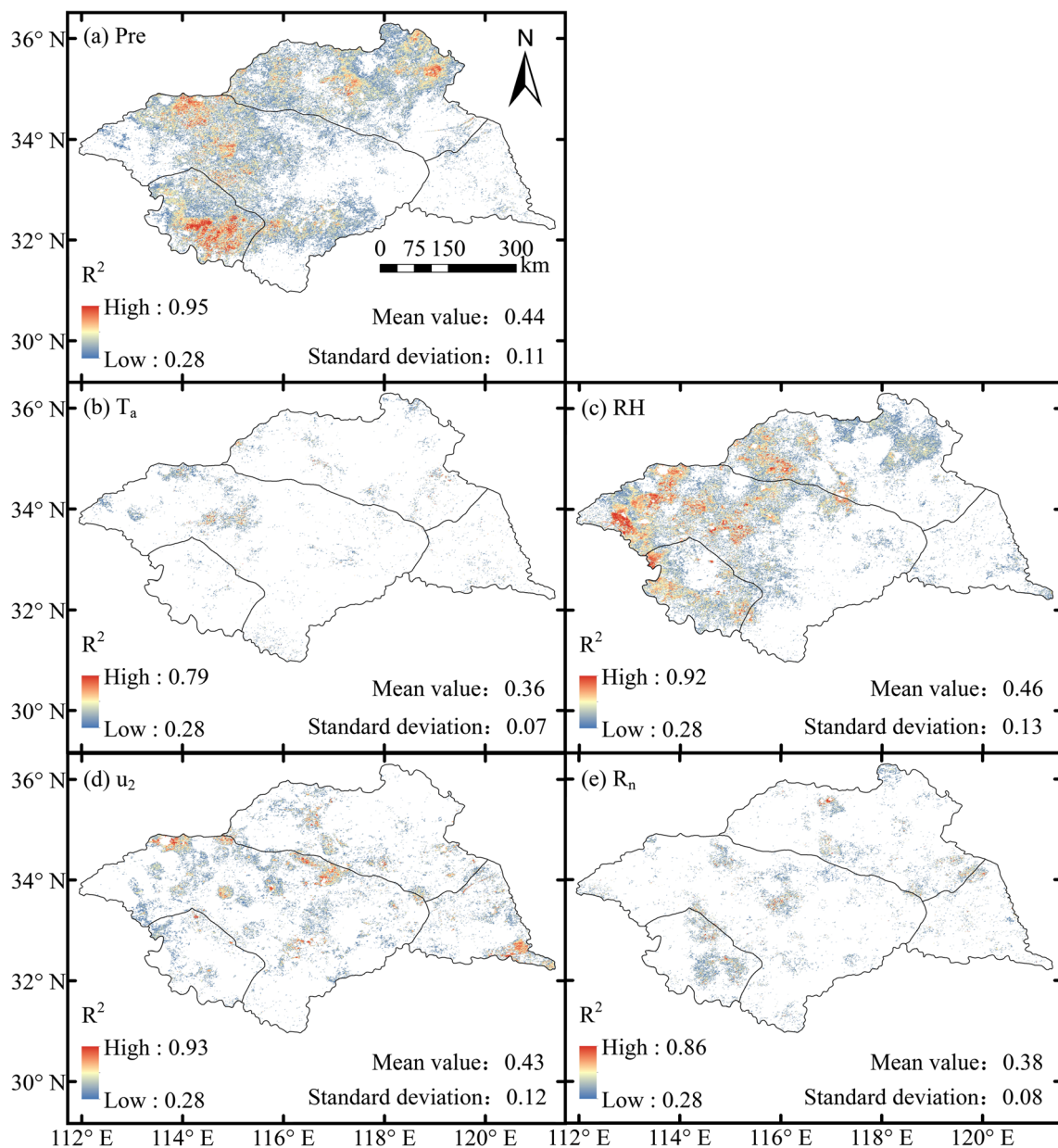


Fig. 12 The correlation between annual ET and corresponding meteorological factors at spatial scale with significance at 0.05.

cycle. The type of land surface affects spatial and temporal variations of ET (Dias et al. 2015; Douglas et al. 2009; Olchev et al. 2008). In our study, the magnitude of ET of different land-use types followed in the order of forests>grasslands>croplands>wetlands>water bodies>urban/built-up areas>barren. This result is basically consistent with the findings of Deng et al. (2017), Zhang et al. (2018a), and Huang et al. (2019). The possible reasons for the large amount of ET of forests are that (a) physiological characteristics of forest root water absorption for transpiration and (b) the contribution of low plants under the canopy of forest with high density to the overall ET of forest.

Future studies and uncertainty

Our study quantitatively assessed the impacts of climate change and LUCC on ET through different input remote sensing data of ET product and land cover types product. The utilization of remote sensing data will bring some inaccuracies and uncertainties into our research unavoidably. The temporal incorrectness may come from the temporal inaccuracies of the remote sensing dataset. Under this situation, further research should be carried out using multi-source climatic dataset and surface ET data to improve the accuracy and strengthen the eventual conclusions. We explored LUCC and their impacts

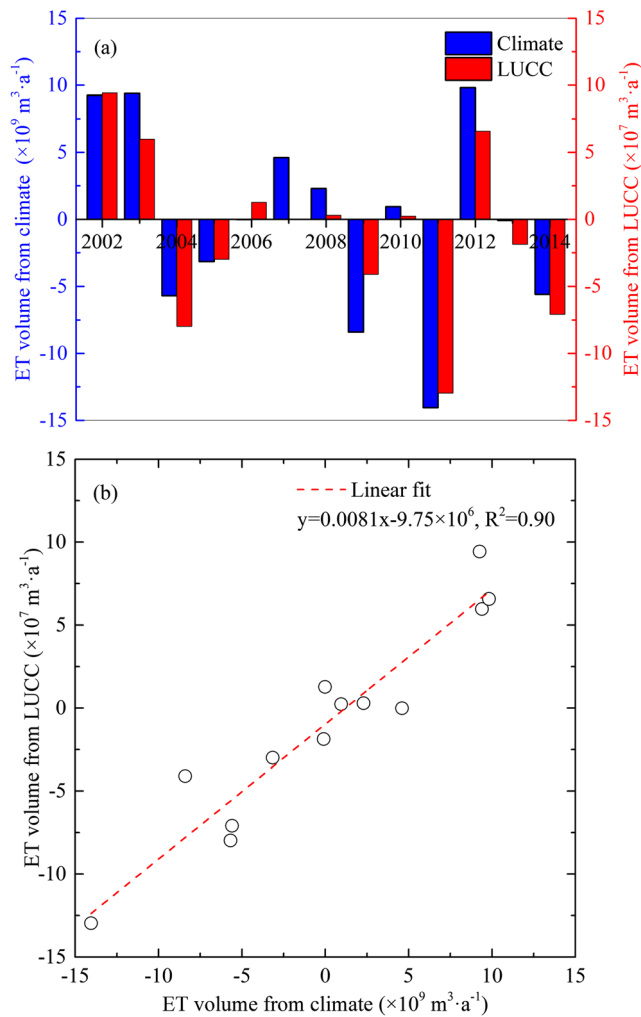


Fig. 13 ET volume from climate and LUCC (a) and their linear fit (b)

on ET in our study. However, how to quantify the contribution of each land-use change type to ET precisely remains to be further studied and discussed. Moreover, the regional impacts of land-use types such as reforestation via influencing atmospheric moisture, Pre, and energy balance in the HRB are still unclear. Meteorological factors can affect land-use types, and in turn, land-use types can also influence the local climate. The interactions between the meteorological factor and land-use types can lead to substantial uncertainty in their roles in affecting ET. Future research based on regional land surface models should take into consideration the relation between the contributions of climate change and LUCC.

Conclusions

This study utilized remote sensing and meteorological datasets to estimate surface ET and variations under different

land-use types in the HRB. The impacts of climate change (meteorological factors) and human activities (LUCC) on surface ET were investigated. The spatiotemporal variation characteristics of ET, the variation trend of land-use types, ET variation characteristics of different land cover types, and the influence of LUCC and climate change on ET of the HRB in the nearly 14-years were discussed. Specific research outcomes are as follows:

Compared with the annual ET estimated by the water balance method and monthly ET by EC measurements as well as E_{pan} data, the MOD16 product data is more accurate and can be used to estimate the ET of the HRB. Except for the slight increase of ET in spring, ET in other seasons of the HRB showed decreasing trends, especially significant in winter ($p < 0.05$). The land-use type of the HRB is mainly croplands, the areas with higher elevations in the southwest and northwest HRB are covered by forests and grasslands, and some areas in lower HRB are also covered by grasslands. The croplands area decreased at a rate of $-176.2 \text{ km}^2 \cdot \text{a}^{-1}$, which was mainly transformed into grasslands and urban/built-up. The forests area increased at a rate of $40.9 \text{ km}^2 \cdot \text{a}^{-1}$ and was mainly transformed from grasslands. The overall grasslands area presented a w-type fluctuation and decreased at the rate of $-35.8 \text{ km}^2 \cdot \text{a}^{-1}$, and the transformed land-use area was in order: croplands>forests>wetlands>urban/built-up>barren>water bodies. The average annual ET in the HRB is closely related to the land-use types, and there are substantial differences in ET among different land-use types, all demonstrating obvious downward trends. The annual ET showed in the following order: forests>grasslands>croplands>wetlands>water bodies>urban/built-up>barren. In terms of meteorological factors, the main controlling factors that finally influence the ET decrease may be the water conditions (Pre decrease and RH decrease) in this basin. Overall, the LUCC has a smaller influence on ET than climate change in the HRB.

The analysis contributed important understanding of ET changes and revealed the impacts of climate change and LUCC on ET, which will assist water managers to predict expected effects, reduce uncertainties, and provide a foundation for sustainable water use management.

Acknowledgments This research was supported by the Anhui Provincial Natural Science Foundation (1908085QD171); National Natural Science Foundation of China (41905100), Anhui Agricultural University Science Foundation for Young Scholars (2018zd07), Anhui Agricultural University Introduction and Stabilization of Talent Fund (yj2018-57), National Key Research and Development Program of China (2018YFD0300905), Scientific Research Project of Anhui Meteorological Bureau (KM202003), and Postgraduate Research and Practice Innovation Program of Jiangsu Province (KYCX17_0885).

Compliance with ethical standards

Conflicts of interest The authors declare that they have no conflict of interest.

References

- Bastiaanssen WGM, Menenti M, Feddes RA, Holtslag AAM (1998a) A remote sensing surface energy balance algorithm for land (SEBAL): 1. Formulation. *J Hydrol* 212-213:198–212
- Bastiaanssen WGM, Pelgrum H, Wang J, Ma Y, Moreno JF, Roerinka GJ, Tvd W (1998b) A remote sensing surface energy balance algorithm for land (SEBAL): Part 2: Validation. *J Hydrol* 212-213:213–229
- Boisier JP, Noblet-Ducoudré N, Ciais P (2014) Historical land-use-induced evapotranspiration changes estimated from present-day observations and reconstructed land-cover maps. *Hydrol Earth Syst Sci* 18(9):3571–3590
- Brath A, Montanari A, Moretti G (2006) Assessing the effect on flood frequency of land use change via hydrological simulation (with uncertainty). *J Hydrol* 324:141–153
- Bronstert A, Niehoff D, Bürger G (2002) Effects of climate and land-use change on storm runoff generation: present knowledge and modelling capabilities. *Hydrol Process* 16:509–529
- Chu R, Li M, Shen S, Islam ARMT, Cao W, Tao S, Gao P (2017) Changes in reference evapotranspiration and its contributing factors in Jiangsu, a major economic and agricultural province of Eastern China. *Water* 9:486
- Chu R, Li M, Islam ARMT, Fei D, Shen S (2019) Attribution analysis of actual and potential evapotranspiration changes based on the complementary relationship theory in the Huai River basin of eastern China. *Int J Climatol* 39(10):4072–4090
- Costa MH, Botta A, Cardille JA (2003) Effects of large-scale changes in land cover on the discharge of the Tocantins River, Southeastern Amazonia. *J Hydrol* 283:206–217
- Deng X, Liu Y, Liu Z, Yao J (2017) Temporal-spatial dynamic change characteristics of evapotranspiration in arid region of Northwest China. *Acta Ecol Sin* 37(9):2994–3008
- Dias L, Macedo M, Costa M, Coe M, Neill C (2015) Effects of land cover change on evapotranspiration and streamflow of small catchments in the upper Xingu river basin, central Brazil. *J Hydrol Reg Stud* 4: 108–122
- Douglas EM, Jacobs JM, Sumner DM, Ray RL (2009) A comparison of models for estimating potential evapotranspiration for Florida land cover types. *J Hydrol* 373:366–376
- Fan J, Li D, Gao M (2014) Spatio-temporal variations of evapotranspiration in Shaanxi province using MOD16 products. *Ecol Environ Sci* 23(9):1536–1543
- Feng F, Yao Y, Zhang Y, Li X (2015) Spatio-temporal variations of evapotranspiration in Sanjiang plain using MOD16 products. *Ecol Environ Sci* 24(11):1858–1864
- Feng X, Fu B, Piao S, Wang S, Ciais P, Zeng Z (2016) Revegetation in China's Loess Plateau is approaching sustainable water resource limits. *Nat Clim Chang* 6:1019–1022
- Gong T, Lei H, Yang D, Jiao Y, Yang H (2017) Monitoring the variations of evapotranspiration due to land use/cover change in a semiarid shrubland. *Hydrol Earth Syst Sci* 21:863–877
- Gowda PH, Chavez JL, Colaizzi PD, Evett SR, Howell TA, Tolck JA (2008) ET mapping for agricultural water management: present status and challenges. *Irrig Sci* 26:223–237
- Han J, Zhao Y, Wang J, Zhang B, Zhu Y, Jiang S, Wang L (2019) Effects of different land use types on potential evapotranspiration in the Beijing-Tianjin-Hebei region, North China. *J Geogr Sci* 29(6): 922–934
- He Y, Ye J, Yang X (2015) Analysis of the spatio-temporal patterns of dry and wet conditions in the Huai River Basin using the standardized precipitation index. *Atmos Res* 166:120–128
- Huang K, Lu Y, Wei Z, Chen H, Zhang B, Ma W (2019) Effects of land use and climate change on spatiotemporal changes of evapotranspiration in Haihe River Basin. *J Geogr Sci* 21(12):1888–1902
- Jung M, Reichstein M, Ciais P, Seneviratne SI, Sheffield J, Goulden ML (2010) Recent decline in the global land evapotranspiration trend due to limited moisture supply. *Nature* 467:951–954
- Kundu S, Khare D, Mondal A (2017) Past, present and future land use changes and their impact on water balance. *J Environ Manag* 197: 582–596
- Lettenmaier DP, Famiglietti JS (2006) Hydrology: Water from on high. *Nature* 444:562–563
- Li M, Chu R, Shen S, Islam ARMT (2018a) Quantifying climatic impact on reference evapotranspiration trends in the Huai River Basin of Eastern China. *Water* 10:144
- Li M, Chu R, Shen S, Islam ART (2018b) Dynamic analysis of pan evaporation variations in the Huai River Basin, a climate transition zone in eastern China. *Sci Total Environ* 625:496–509
- Li M, Chu R, Arnt I, Jiang Y, Shen S (2020) Estimating daily actual evapotranspiration of a rice-wheat rotation system in typical farmland in the Huai River Basin using a two-step model and two one-step models. *J Integr Agric*. [https://doi.org/10.1016/S2095-3119\(20\)63223-3](https://doi.org/10.1016/S2095-3119(20)63223-3)
- Liu M, Hu D (2019) Response of wetland evapotranspiration to land use/cover change and climate change in Liaohe River Delta, China. *Water* 11:955
- Liu W, Hong Y, Khan SI, Huang M, Vieux BE, Caliskan S, Grout T (2010) Actual evapotranspiration estimation for different land use and land cover in urban regions using Landsat 5 data. *J Appl Remote Sens* 4(1):041873. <https://doi.org/10.1117/1.3525566>
- Ma Z, Yan N, Wu B, Stein A, Zhu W, Zeng H (2019) Variation in actual evapotranspiration following changes in climate and vegetation cover during an ecological restoration period (2000–2015) in the Loess Plateau, China. *Sci Total Environ* 689:534–545
- Mann HB (1945) Nonparametric test against trend. *Econometrica* 13(3): 245–259
- Menz MHM, Dixon KW, Hobbs RJ (2013) Hurdles and opportunities for landscape-scale restoration. *Science* 339:526–527
- Miralles DG, Holmes TRH, Jeu RAMD, Gash JH, Meesters AGCA, Dolman AJ (2011) Global land-surface evaporation estimated from satellite-based observations. *Hydrol Earth Syst Sci* 15:453–469
- Mu Q, Zhao M, Running SW (2011) Improvements to a MODIS global terrestrial evapotranspiration algorithm. *Remote Sens Environ* 115: 1781–1800
- Norman JM, Kustas WP, Humes KS (1995) Source approach for estimating soil and vegetation energy fluxes in observations of directional radiometric surface temperature. *Agric For Meteorol* 77:263–293
- Odongo VO, Oel PR, Tol C, Su Z (2019) Impact of land use and land cover transitions and climate on evapotranspiration in the Lake Naivasha Basin, Kenya. *Sci Total Environ* 682:19–30
- Olchev A, Ibrom A, Priess J, Erasmi S, Leemhuis C, Twele A, Radler K, Kreilein H, Panferov O, Gravenhorst G (2008) Effects of land-use changes on evapotranspiration of tropical rain forest margin area in Central Sulawesi (Indonesia): modelling study with a regional SVAT model. *Ecol Model* 212(1-2):131–137
- Roderick ML, Hobbins MT, Farquhar GD (2009) Pan evaporation trends and the terrestrial water balance. II. Energy balance and interpretation. *Geogr Compass* 3:761–780
- Roerink GJ, Su Z, Menenti M (2000) S-SEBI: A simple remote sensing algorithm to estimate the surface energy balance. *Phys Chem Earth Part B* 25:147–157
- Sánchez JM, Kustas WP, Caselles V, Anderson MC (2008) Modelling surface energy fluxes over maize using a two-source patch model and radiometric soil and canopy temperature observations. *Remote Sens Environ* 112:1130–1143
- Sen PK (1968) Estimates of the regression coefficient based on Kendall's Tau. *J Am Stat Assoc* 63(324):1379–1389
- Shan N, Shi Z, Yang X, Gao J, Cai D (2015) Spatiotemporal trends of reference evapotranspiration and its driving factors in the Beijing-

- Tianjin Sand source control project region, China. *Agric For Meteorol* 200:322–333
- Stanhill G, Cohen S (2001) Global dimming: a review of the evidence for a widespread and significant reduction in global radiation with discussion of its probable causes and possible agricultural consequences. *Agric For Meteorol* 107:255–278
- Su Z (2002) The Surface Energy Balance System (SEBS) for estimation of turbulent heat fluxes. *Hydrol Earth Syst Sci* 6:85–99
- Theil H (1950) A rank invariant method of linear and polynomial regression analysis. *Wetenschappen, Nederlandse Akademie Van*
- Tian H, Wu Q, Tong Y (2011) Evaluation on energy balance of farmland in Shouxian county of Anhui province. *J Appl Meteorol Sci* 22(3): 356–361
- Vörösmarty CJ, Sahagian D (2000) Anthropogenic disturbance of the terrestrial water cycle. *Bioscience* 50:753–765
- Vörösmarty CJ, Green P, Salisbury J, Lammers RB (2000) Global water resources: vulnerability from climate change and population growth. *Science* 289(5477):284–288
- Walter MT, Wilks DS, Parlange JY, Schneider RL (2004) Increasing evapotranspiration from the conterminous united states. *J Hydrometeorol* 5(3):405–408
- Wang G, Zhang Y, Liu G, Chen L (2006) Impact of land-use change on hydrological processes in the Maying River basin, China. *Sci China Earth Sci* 49:1098–1110
- Wang P, Yan J, Jiang C, Cao Y (2016) Spatial and temporal variations of evapotranspiration and its influencing factors in the Loess Plateau in Shaanxi-Gansu-Ningxia region. *J Desert Res* 36(2):499–507
- Wang F, Wang Z, Zhang Y, Shen F (2018) Spatio-temporal variations of evapotranspiration in Anhui province using MOD16 products. *Resour Environ in the Yangtze Basin* 27(3):523–534
- Wang H, Xiao W, Zhao Y, Wang Y, Hou B, Zhou Y, Yang H, Zhang X, Cui H (2019) The spatiotemporal variability of evapotranspiration and its response to climate change and land use/land cover change in the three Gorges reservoir. *Water* 11(9):1739
- Waring RH, Running SW (2007) *Forest ecosystems: analysis at multiple scales*. Elsevier Academic Press
- Wu G, Liu Y, Zhao X, Ye C (2013) Spatio-temporal variations of evapotranspiration in Poyang Lake Basin using MOD16 products. *Geogr Res* 32(4):617–627
- Xu L, Shi Z, Wang Y, Zhang S, Chu X, Yu P, Xiong W, Zuo H, Wang Y (2015) Spatiotemporal variation and driving forces of reference evapotranspiration in Jing River Basin, northwest China. *Hydrol Process* 29:4846–4862
- Yan J, Yu J, Tao G, Vos J, Bouman BAM, Xie G, Meinke H (2010) Yield formation and tillering dynamics of direct-seeded rice in flooded and nonflooded soils in the Huai River Basin of China. *Field Crop Res* 116(3):252–259
- Ye H, Zhang T, Yi G, Li J, Bie X, Liu D, Luo L (2018) Spatio-temporal characteristics of evapotranspiration and its relationship with climate factors in the source region of the Yellow River from 2000 to 2014. *Acta Geograph Sin* 73(11):2117–2134
- Zhang M, Zeng Y, Qi Y (2018) Analyzing spatio-temporal variations of evapotranspiration in Dongting Lake Basin during 2000–2014 based on MOD16. *Trans CSAE* 34(20):160–168
- Zhang T, Liu J, Dong X, Wang H, Sun Z, Tan X, Cheng X (2018b) Spatiotemporal variation of evapotranspiration in Huan River Basin using the MOD16 dataset. *J Irrig Drain* 37(8):121–127
- Zhao J, Chen X, Zhang J, Zhao H, Song Y (2017) Higher temporal evapotranspiration estimation with improved SEBS model from geostationary meteorological satellite data. *Sci Rep* 9:14981
- Zou M, Niu J, Kang S, Li X, Lu H (2017) The contribution of human agricultural activities to increasing evapotranspiration is significantly greater than climate change effect over Heihe agricultural region. *Sci Rep* 7:8805

Publisher's note Springer Nature remains neutral with regard to jurisdictional claims in published maps and institutional affiliations.